Methylammonium fragmentation in amines as source of localized trap levels and the healing role of Cl in hybrid lead-iodide perovskites

Pietro Delugas,[1,2] Alessio Filippetti,[2,*] and Alessandro Mattoni[2,†]
[1]*CompuNet, Istituto Italiano di Tecnologia, Via Morego 30, 16163 Genova, Italy*
[2]*Istituto Officina dei Materiali, CNR-IOM Cagliari SLACS, Cittadella Universitaria, I-09042 Monserrato (CA), Italy*
(Received 8 May 2015; published 2 July 2015)

The resilience to deep traps and localized defect formation is one of the important aspects that qualify a material as a suited photoabsorber in solar cell devices. Here we investigate by *ab initio* calculations the fundamental physics and chemistry of a number of possible localized defects in hybrid methylammonium lead-iodide perovskites. Our analysis encompasses a number of possible molecular fragments deriving from the dissociation of methylammonium. In particular, we found that in stoichiometric conditions both ammonia and methylamine molecules present lone-pair localized levels well within the perovskite band gap, while the radical cation $CH_2NH_3^+$ observed by EPR after irradiation injects partially-occupied levels into the band gap but only in *p*-type conditions. These defects are thus potentially capable of significantly altering absorption and recombination properties. Amazingly, we found that additional interstitial Cl is capable of removing these localized states from the band gap. These results are consistent with the observed improvement of photoabsorption properties due to the Cl inclusion in the solution processing.

DOI: 10.1103/PhysRevB.92.045301 PACS number(s): 71.55.−i, 78.20.−e, 82.50.Hp, 88.40.fh

I. INTRODUCTION

The outstanding photoconversion properties of $CH_3NH_3PbI_3$ perovskites (we will, from now on, abbreviate methylammonium as M and methylammonium lead iodide as $MPbI_3$) have been the subject of an impressive number of experimental and theoretical studies in the last few years [1–6]. Nowadays, most of the key ingredients which characterize the photoabsorption properties of the system, at least in its bulk form, are understood: the large absorption coefficient in the important frequency range [7–11], the dominance of unbound electron-hole recombination over excitonic effects at room temperature [12,13], the small band-to-band radiative recombination rate [8,14], the long ($\approx 10^2$–10^3 ns) lifetime, and diffusion length (hundreds nm) [2,12,13,15,16].

In summary, the great appeal of this system stems from the fact that, while processed through low-cost solid solution as organic materials, it is nevertheless assignable, for what concerns photoabsorption properties, to the category of the best crystalline semiconducting absorbers (see Refs. [7–9] for a detailed comparison with GaAs).

However, several aspects are still not fully understood. One of them concerns the incidence and typology of native defects present in these materials. The fact that these films prepared at low thermal budgets have optimal optical absorption is a clear indication of the resilience of the electronic properties against structural defects and vacancies [17].

Experiments provide few specific indications about point defects and intragap electronic levels. Electronic paramagnetic resonance (EPR) measurements detect $CH_2NH_3^+$ cations and Pb^0 paramagnetic clusters in samples which had been irradiated with intense ultraviolet light [18]. Evidence of Pb metallic clusters in $MPbI_3$ is also given by x-ray photoemission spectroscopy [19,20]; Ref. [19] reports also the presence of occupied (mainly in *n*-type conditions) or empty (mainly in *p*-type conditions) intragap electronic levels distributed at variable energies inside the gap.

Indirect information about intragap electronic levels can also be drawn from photoluminescence (PL) experiments. As an example, a recent paper [12] revealed that while transient PL spectroscopy in the high excitation density regime is dominated by unbound electron-hole radiative recombination, the steady-state PL intensity follows a 3/2-power law as a function of laser intensity ($PL \propto I^{3/2}$) which deviates from a purely radiative behavior ($PL \propto I$) and suggests the presence of intragap states. These intragap states can trap either electrons or holes, but not both of them simultaneously, thus indicating that these traps should be either fully occupied or empty but not partially filled. The trapping contribution is visible up to an injected carrier density of $\sim 10^{16}$–10^{17} cm^{-3}, above which the radiative regime takes place and the linear behavior $PL \propto I$ is recovered.

First-principles calculations are an extremely useful approach to evaluate the presence of defects in the systems. In several recent theoretical papers [21–23] (see also Refs. [9,10] for a review) the most common point defects (vacancies, interstitials, substitutionals, and anti-sites) were thoroughly analyzed. It was found that the defects with the lowest formation energies (Pb vacancy and interstitial methylammonium, according to Ref. [15]) are shallow acceptors and donors, respectively, thus coherently with the expectation of good *p*-type or *n*-type conductivity and recombination properties dominated by radiative processes.

For some defects with larger formation energies (e.g., Pb interstitial and antisite [15,22,24]) it is estimated by the very simplified transition-state argument that electronic levels lying well into the band gap could occur, but no explicit evidence of these defects was obtained from the calculated electronic properties.

In the search for localized states evidenced by PL, in this paper we use density functional theory calculations to analyze a different scenario, i.e., the possibility of intragap electronic localization induced by the presence of interstitial molecules

*Corresponding author: alessio.filippetti@dsf.unica.it
†Corresponding author: Alessandro.Mattoni@iom.cnr.it

containing a C or N atom with a $2p$ lone pair. We will consider only molecules that derive from the methylammonium dissociation or deprotonation. In doing so, we assume the rather conservative viewpoint of including only moieties that respect the chemical composition and stoichiometry of the bulk perovskite. Apart from the dissociation processes, these and other physically similar impurities can be introduced in $MPbI_3$ accidentally.

Nicely, this limited set of cases is however sufficient to display a significant variety of defect states, whose characteristics are consistent with the PL analysis. In particular, we found that amine groups originating from the lone pair of nitrogen molecules (e.g., ammonia and methylamine produced by M dissociation) have the general tendency to furnish trap states located well into the band gap.

Fragments containing a carbon $2p$ lone pair instead are generally unstable and tend to form bonded complexes with I ions. In this case all the localized electronic states are well below the valence band. This behavior is significantly influenced by the Fermi level position. For example in p-type conditions the CH_2NH_3 fragment yields one electron to (captures one hole from) the valence band and loosens its bond with iodine. The hole remains thus localized on a C($2p$) state of the fragment. This intragap half-filled level has been actually observed by EPR [18].

Considering these defected perovskites as the starting point, we then include interstitial Cl doping in the analysis (previous calculations [25] only considered Cl as I-substitutional in the bulk perovskite, and as such, hardly capable to change on any significant extent the photoabsorption properties of the perovskite).

Here we give evidence that additional inclusion of 2% interstitial Cl in the perovskite (thus corresponding to p-type conditions) is capable of removing a corresponding fraction of N-derived localized states from the gap without including any additional charge localization in its own. Our results provide clear evidence of the beneficial action of Cl in removing electronic localized states from the gap and furnish a possible explanation to the increase of an order of magnitude in lifetime and diffusion length observed after Cl inclusion in solution.

II. COMPUTATIONAL METHODS

The electronic and structural properties of the defects were computed using the density functional theory within local density approximation, as implemented in the QUANTUM ESPRESSO package [26] which is a well known plane-wave plus ultrasoft pseudopotential [27] code.

As demonstrated by an already vast amount of literature this approach is reliable for computing structural and energetic properties of $MAPbI_3$. LDA (and, in fact, these same pseudopotentials) were previously used [7,8] yielding results which are congruent with those obtained with other functionals and computational techniques [6,10,21,22,28–32].

An accurate treatment of Pb $6p$ states in the conduction band would require the inclusion of spin-orbit coupling [33] (SOC). SOC has in fact small influence on electronic properties of the valence band [30], and in general on energetics and structure of bulk phases or defects. For this reason, even considering the major increase in computational cost required for including SOC in *ab initio* computations, similar to what was done in many other papers on this subject [15,21–23], we choose to discard SOC.

From this choice derives the additional, though not crucial, advantage of the realistic value of the band gap yielded by LDA. As discussed in Ref. [34] this is due to a fortuitous error cancellation. The overestimate of the band gap—due to overlooking SOC—compensates almost exactly for the typical band gap underestimate of most DFT functionals.

Pseudopotentials for I, C, and N have projectors on s and p channels. For C and N the valence reference states are $2s$ and $2p$, and they are $5s$ and $5p$ for iodine. The Pb pseudopotentials have projectors in the s, p, and d channels, with reference valence states $6s$, $6p$, and $5d$. All calculations were done by using a plane-waves basis set cut-off of 35 Ry.

All the reported results are inherent to the same supercell built as a $2 \times 2 \times 1$ repetition of the tetragonal $P4/mbm$ unit cell, containing 4 $MPbI_3$ cubic units, which is the most stable phase at room temperature [35]. This is approximately a $\sqrt{2} \times \sqrt{2} \times 2$ replica of a cubic unit cell. The tetragonal x and y axes correspond to the diagonals of the starting cubic cell.

Periodic boundary conditions are imposed along a tetragonal body centered lattice with vectors $(a,-a,c)$,(a,a,c),$(-a,-a,c)$; in this way the periodic defect lattice is distributed isotropically at a distance equal to the supercell lattice length (17.40 Å). The values of the bulk lattice parameters $a = 8.712$ Å and $c/a = 1.41$ are obtained by the theoretical optimization of the bulk $P4/mbm$ unit cell and are in good agreement with those reported in Ref. [35].

The integrations in the Brillouin zone during self consistency uses a $3 \times 3 \times 3$ Monkhorst-Pack mesh. For the density of states calculation we have used the linear tetrahedron method on an $8 \times 8 \times 8$ k-space mesh.

III. RESULTS AND DISCUSSION

A. Bulk perovskites

In defect-free bulk perovskites, the M^{1+} electronic states are well localized in space, as seen from the calculated DOS in Fig. 1. The electronic structure of methylammonium embedded in the perovskite is not dissimilar to that of the isolated molecule, showing [from bottom, relative to the valence band maximum (VBM)] a singlet (at -19.2 eV) derived from N($2s$)-H($1s$) hybridized states; another singlet at -12.4 eV from C($2s$)-H($1s$) hybridization; a N($2p$)-H($1s$) doublet at -8.8 eV, and another singlet at about -7 eV derived from N($2p$)-C($2p$) states. Finally, the C($2p$)-H($1s$) doublet at -4.8 eV is the HOMO.

Since these states are located well below the VBM, no molecular level interferes directly with the band gap region. The same holds for the empty molecular states (not shown here) being the LUMO well above the conduction band minimum (CBM). This decoupling of extended bands (derived from Pb and I states) with respect to the molecular states does not necessarily hold anymore if we consider configurations with methylammonium broken in C-based or N-based fragments. In the following, we will examine all the possible stoichiometric processes obtained by the fragmentation of methylammonium, giving rise to stable molecules.

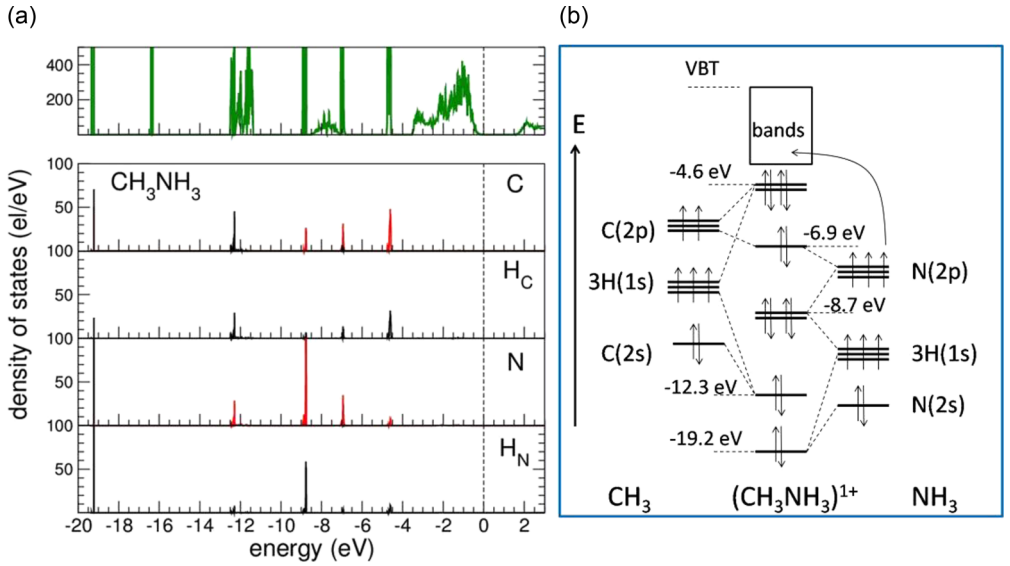

FIG. 1. (Color online) (a) Density of states of bulk $MPbI_3$. The 0 energy is set to the valence band maximum. To better visualize the molecular levels, they are plotted in separate panels, one for each atomic type. Top panel: total DOS (green). Bottom panels: projected DOS on atomic states of methylammonium molecule. HC and HN are hydrogens bound to C and N, respectively; black and red lines refer to *s*-type and *p*-type states. (b) scheme of methylammonium orbital levels, as inferred for the calculated DOS.

B. Methylammonium fragmentation

A neutral M (i.e., not the M^{1+} state of the bulk perovskite) lacks one H to be dissociated in a couple of NH_3 and CH_4 molecules, which would be both stable and neutral. It follows that, forcing a starting configuration with two separated C- and N-based complexes, one of them (the one lacking a hydrogen) will tend to form covalent bonding with neighboring ions, while the most stable will remain located nearby the perovskite A site. For completeness we also include in the analysis the deprotonation processes. Five types of decomposition leaving at least one stable product can be hypothesized: (a) $CH_3NH_3 \rightarrow CH_3 + NH_3$; (b) $CH_3NH_3 \rightarrow CH_4 + NH_2$; (c) $2 \times CH_3NH_3 \rightarrow CH_3NH_2 + NH_4 + CH_3$; (d) $CH_3NH_3 \rightarrow CH_3NH_2 + H$; (e) $CH_3NH_3 \rightarrow CH_2NH_3 + H$.

These five processes conserve the perovskite bulk stoichiometry so that it is possible to estimate their energetic cost by direct comparison of total energies. The results for the completely separated fragments are reported in Table I. The computations show that the CH_3–I fragment has a significant binding energy with NH_3 (0.4 eV) and CH_3NH_2 (0.5 eV).

We should notice that our structures are the product of atomic relaxations which sample a limited portion of the potential energy profile. Thus, we cannot exclude that the same final products could be arranged in a more energetically convenient way than that found in our final state.

TABLE I. Energetic cost of the fragmentation processes(ΔE) examined in this work. The energies are calculated with respect to an equivalent bulk $MPbI_3$ supercell with 16 cubic perovskite units. The corresponding average bond dissociation enthalpies (ΔH) are reported, as a comparison with the corresponding dissociation.

Configuration	ΔE (eV)	ΔH (eV)
$NH_3 + CH_3$–I	2.03	3.17
$CH_4 + NH_2$–I	1.90	3.17
$CH_3NH_2I + NH_4 + CH_3$–I	2.30	3.17
CH_3NH_2I + H–I	2.66	4.03
CH_2NH_3–I + H–I	3.22	4.28

As one can see in Table I the formation energies ΔE substantially reflect the average bond enthalpy ΔH of the C-N bond in case of (a) and (b) configurations (see the Table), and of the N-H bond in the case of (c). Since the dissociation products are stable molecules, they gain some stability at the end of the process, thus ΔE are actually sizably smaller than ΔH.

These large formation energies are indeed coherent with the low concentration of localized defects indicated by the experiments. However, this should not lead to the conclusion that the final products of dissociation are unlikely, since they could form during nonequilibrium solution processing, and not necessarily through the actual thermodynamic dissociation of methylammonium. Further, as reported in Ref. [18] deprotonated fragments are formed upon ultraviolet irradiation and, once created, they are stable.

Finally notice that these results should not be compared with those calculated for point defects in Refs. [9,15,16]: In that case *nonstoichiometric* defects are considered (e.g., vacancies, interstitials, substitutionals) thus a suited choice of atomic chemical potentials can always favor the formation of specific defects. In the present case, all the configurations are stoichiometric, and no chemical reservoir is assumed. The resulting energies depend only on the actual energetic cost of the dissociation mechanism and do not depend on adjustable parameters. In the following we will analyze structural and electronic properties of the fragments.

C. Dissociation of methylammonium in ammonia and iodomethane

Following the mechanism (a) we forced the separation of one M in NH_3 (ammonia) and CH_3. The former remains close

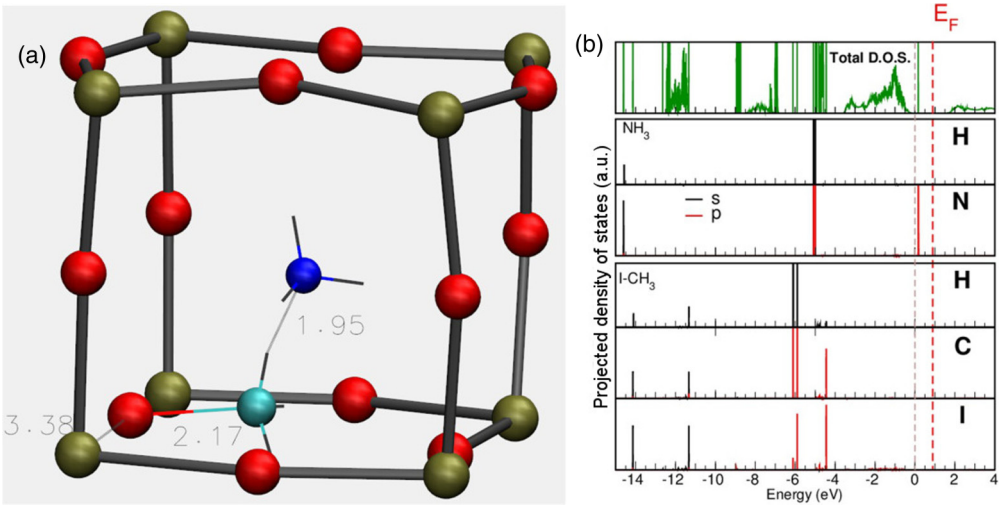

FIG. 2. (Color online) Atomic and electronic structure of the perovskite after $CH_3NH_3 \rightarrow CH_3 + NH_3$ (a) dissociation process. (a): Atomic structure in close-by configuration: CH_3 migrates onto a PbI_4 plaquette to form a iodomethane molecule (CH_3I, the CI dimer indicated by cyan and red balls), while NH_3 remains close to the initial A-site of the perovskite. (b): corresponding DOS. Upper panel: total DOS (green); lower panels: atom-resolved DOS for CH_3I and NH_3 molecules (orbital contribution labels are the same as the DOS in Fig. 1). We take the VBM as the reference 0 energy. E_F is placed at the middle between the highest occupied level and the CBM.

to the starting M position (i.e., the A site of the perovskite) and fairly stable in its ground state, with three electrons distributed in an equal number of N-H bonds, and other two in a lone-pair HOMO of N($2p$) orbital character. On the other hand, CH_3 is in a highly electronegative state; it migrates toward an I atom (also in need of an electron to fill the valence hole, assuming a neutral M at the start).

After structural optimization, a stable CH_3-I complex (*"methyl-iodide,"* also called *"iodomethane"*) is established, with the C-I axis lying nearly parallel to the PbI_4 square and a bond length of 2.17 Å. The key feature, for what concerns the photoabsorption properties, is that the N($2p$) HOMO level of NH_3 is high enough in energy to overcome the whole I($5p$)-Pb($6s$) valence band manifold (spanning a 3.6 eV wide energy interval) and intrudes well within the band gap. Thus, a doubly occupied donor appears 0.17 eV above the VBM.

For iodomethane, on the other hand, the HOMO state is a highly stable I($5p$)-C($2p$) σ-bond lying well below the valence band manifold, thus ineffective for what concerns the band gap region. The detailed properties of this configuration are shown in Fig. 2.

D. Dissociation of methylammonium in methane and iodoamine

Following mechanism (b) we separate methylammonium in CH_4 (methane) and NH_2; the behavior of C and N is exchanged with respect to the previous case: The stable methane molecule remains nearby the starting M site, while NH_2 migrates toward a I ion and forms a NH_2I (iodoamine) molecule, again placed at the interstice of the perovskite's octahedral cage [36].

The electronic structure of CH_4 (shown in Fig. 3) is quite close to that of an isolated methane molecule, indicating small interaction with the inorganic surroundings. However, the electronic levels of this fragment remain far from the important energy region of photoabsorption.

The interstitial NH_2I fragment also shows an electronic structure substantially similar to that of the isolated iodoamine molecule, with the LUMO given by a N($2p$)-I($5p$) hybridized state lying just at the bottom of the conduction band. Thus, this state is a deep acceptor, but with a binding energy too small to be effective as recombination center.

E. Formation of ammonium, iodomethane, and methylamine

Following dissociation process (c), specularly to path (b), we separate the methylammonium in NH_4 and CH_2 fragments. Again the stable NH_4 remains at the A site and the unstable fragment is attracted by one I ion. In this case the CH_2 not only binds to a I ion but—as it has to stabilize two $2p$ lone pairs—captures also one H from a close-by methylammonium (thus ending up to a methylamine) and forms a stable CH_3–I *iodomethane* complex. This result confirms that the formation of $2p$ lone pair on N is energetically more favorable with respect to C.

Structural and electronic properties of methylamine and iodomethane are illustrated in the discussion of dissociation paths (b) and (d), respectively. The four electronic levels stemming from ammonium valence states are all well below the I($5p$) valence band with 1 level at about -20 eV and three almost degenerate levels at about -10 eV with respect to the VBM.

F. Dissociation of methylammonium in hydrogen iodide and methylamine.

The methylamine can also form directly from the deprotonation process of path (d). The detached H migrates toward the PbI_6 octahedron and binds to an I to form a HI molecule (hydrogen iodide) [36]. The deprotonated CH_3NH_2 (methylamine) molecule is stable (structural and electronic

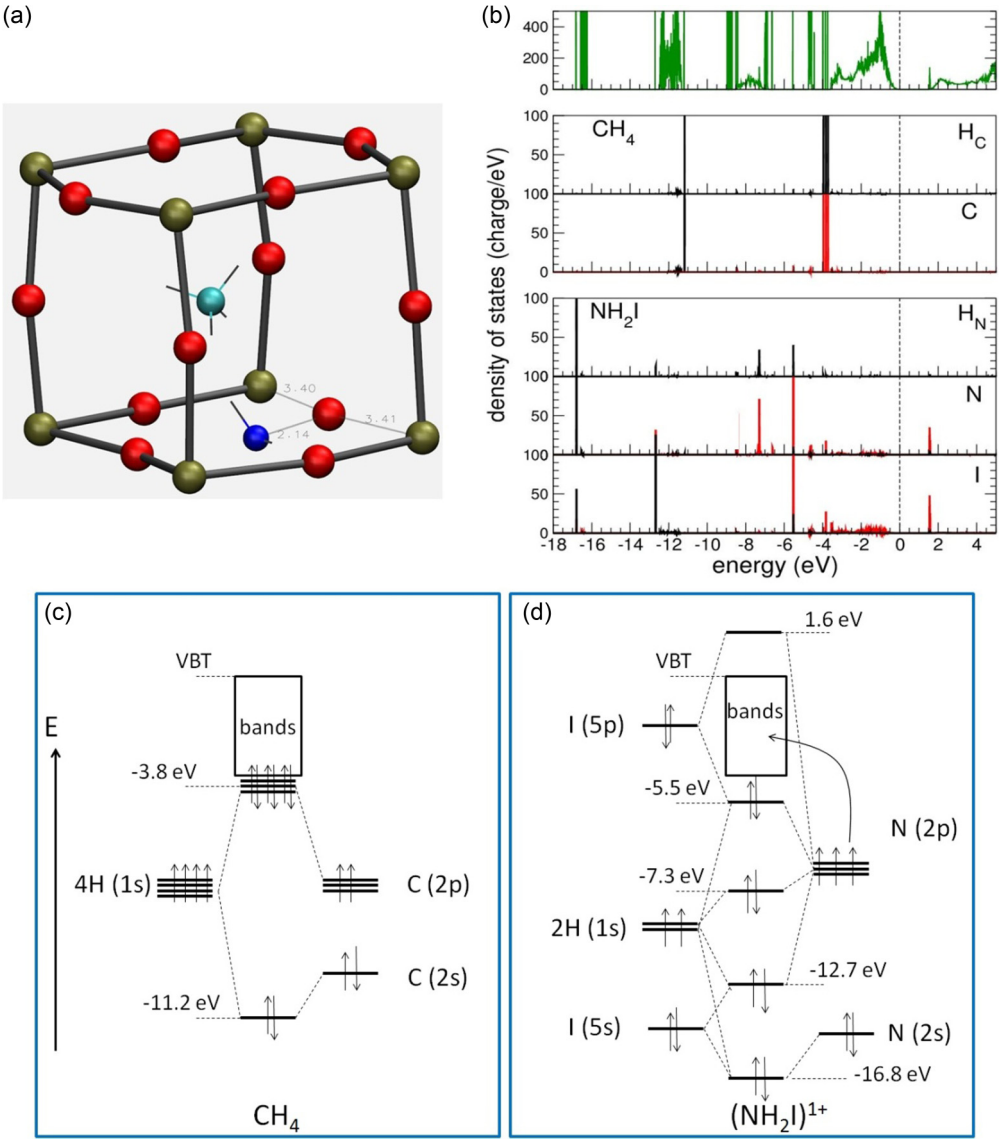

FIG. 3. (Color online) Structural optimization of the $CH_3NH_3 \rightarrow CH_4 + NH_2$ dissociation (c); (a) NH_2 migrates into a PbI_4 plaquette to form a iodoamine like complex (NH_2–I), and methane (CH_4) remains stuck to the starting M site. (b): corresponding DOS, and atomic projected DOS. Orbital types and labels are the same as in Fig. 2. Reference 0 energy is placed at the VBM. (c) and (d): schemes of the molecular levels, as inferred from the atomic-projected DOS.

properties are shown in Fig. 4) and thus remains in a substitutional position at the A site.

At variance with M, methylamine is neutral, thus the I($5p$) valence band manifold remains nominally hole doped. Our calculations show that this hole is compensated by the HI formation, which produces localized s–p states, thus formally subtracting one I to the I($5p$) bands. But the most interesting aspect is that the filled methylamine HOMO and the empty hydrogen iodide LUMO are both located well within the band gap.

For what concerns methylamine, its 14 electrons fill 7 doubly-occupied localized levels. The second highest in energy (a C-H bond at -2.9 eV) falls well within the I($5p$) valence manifold, and it is slightly broadened and barely visible on the same scale of the other levels of the molecule (*see the DOS enlargement in a small energy region around the band gap in Fig. 4(b)*).

The highest occupied state of methylamine is a N($2p$) lone pair, located 1.17 eV above the VBM; thus, as in the case of the the ammonia molecule, we have a stable molecule whose HOMO, derived by a lone pair of N($2p$) character, is high enough in energy to emerge above the VBM.

For what concerns the HI molecule, it presents a I($5p$)-H($1s$) singlet at -6.2 eV, and a I($5p$)-H($1s$) doublet at -3.9 eV. Interestingly, its first empty state is another I($5p$)-H($1s$) bond below the CBM. To highlight the characteristics of these in-gap states we also calculated the band dispersion along the Γ-Z direction [Fig. 4(c)]: while the CH_3NH_2 HOMO is quite flat through the whole region, the HI LUMO is characterized by a substantial broadening ($\approx$0.1 eV), remaining however separated from the CBM by $\sim$50 meV. The presence of these fully occupied and empty in-gap states is a potentially relevant feature for what concerns photoabsorption and photoemission,

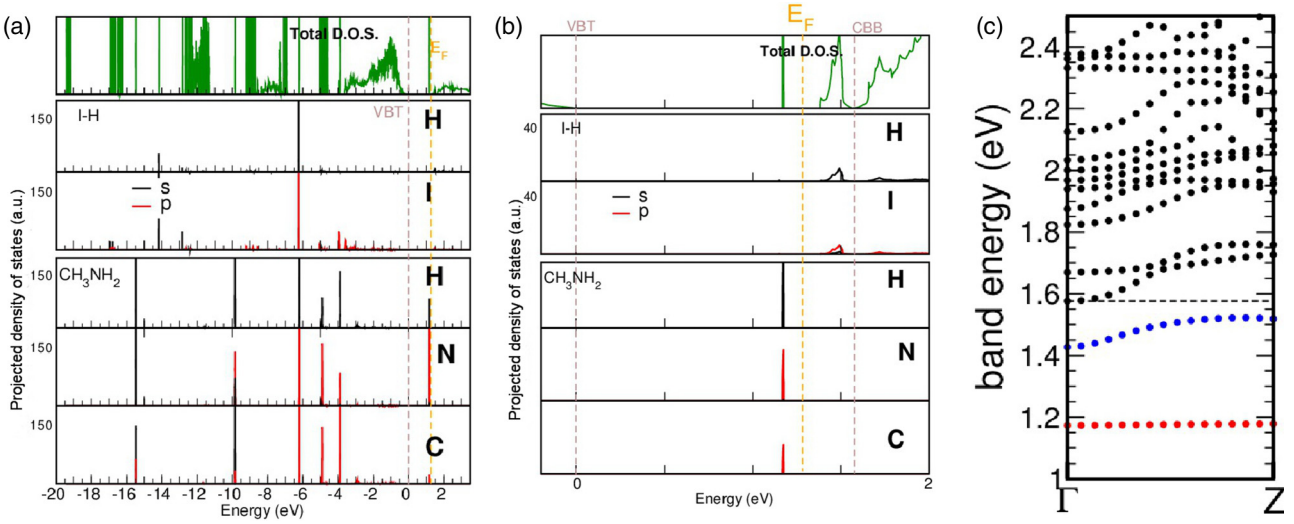

FIG. 4. (Color online) Simulation of the $CH_3NH_3 \rightarrow CH_3NH_2 + H-I$ dissociation: one H migrates into a PbI_6 octahedron to form hydrogen iodide (HI), leaving a stable methylamine molecule (CH_3NH_2) close to the original M-site. (a): Atomic resolved DOS in the full energy range. The 0 reference energy is placed at the VBM; E_F is placed at the middle between occupied and empty states. Orbital types and labels are the same as in Fig. 1(a). (b) DOS in a small energy interval around the band gap, to better visualize the molecular levels overlapping with the valence bands (see text). (c): Band structure along the $\Gamma-Z$ direction. The flat red band is due to the N($2p$) lone-pair levels of methylamine. The blue band is related to H-I empty levels. The dashed line indicates the level of the conduction band bottom.

since they represent sources of strong nonradiative electron-hole recombination processes.

G. Dissociation of methyl-ammonium in hydrogen iodide and CH_2NH_3–I

Following process (e) the deprotonation occurs at the C side. We have again the formation of an H-I dimer which implies the transfer of one electron to the I($5p$) valence band. The deprotonated methyl-ammonium fragment is thus neutral. At variance with the CH_3NH_2 fragment, CH_2NH_3 binds to an I ion and forms a stable complex which is in many aspects analogous to the CH_3–I complex seen above. Also the computed bond length (2.17 Å) is the same as we obtained for the iodomethane complex.

All of the 14 electrons of this fragment are localized in molecular levels whose energies are well below the valence band (see Fig. 5). With respect to the valence band top (VBM) we have 3 distinct levels at −14 eV, −9.5 eV, and −6 eV; we have four more electronic levels that are organized in two

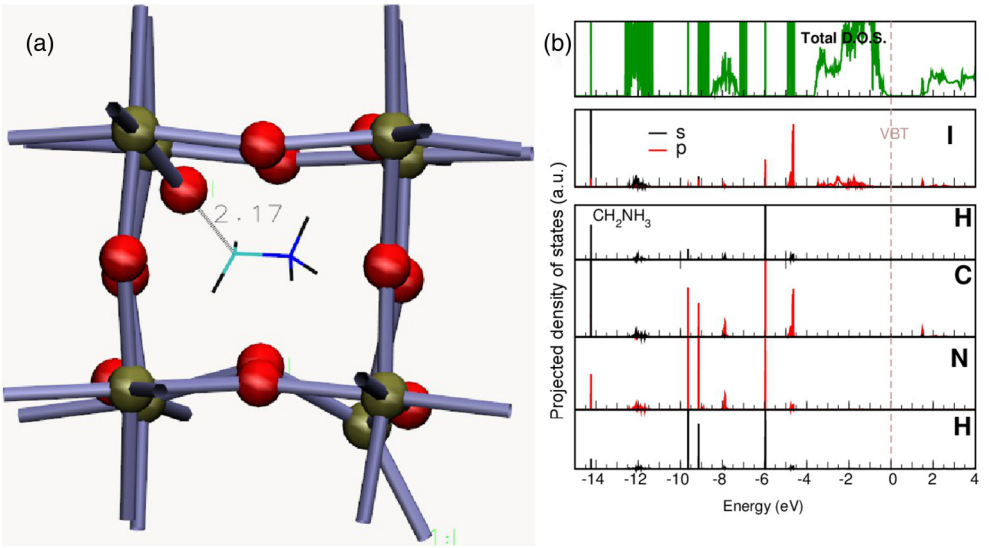

FIG. 5. (Color online) (a) Structure of the CH_2NH_3–I complex. The I ion is displaced from its equilibrium position to bind to the deprotonated fragment. (b) electronic structure of the CH_2NH_3–I complex, illustrated by the DOS projected on CH_2NH_3 and I sites. States are filled up to the valence band minimum (VBM) which is placed at 0. Except for the H-I peak close to the conduction band there are no other defect states within the gap. Five distinct peaks (*see text*) are present in the projected DOS of CH_2NH_3; C-derived $s-p$ states are strongly hybridized with the I $5p$ states.

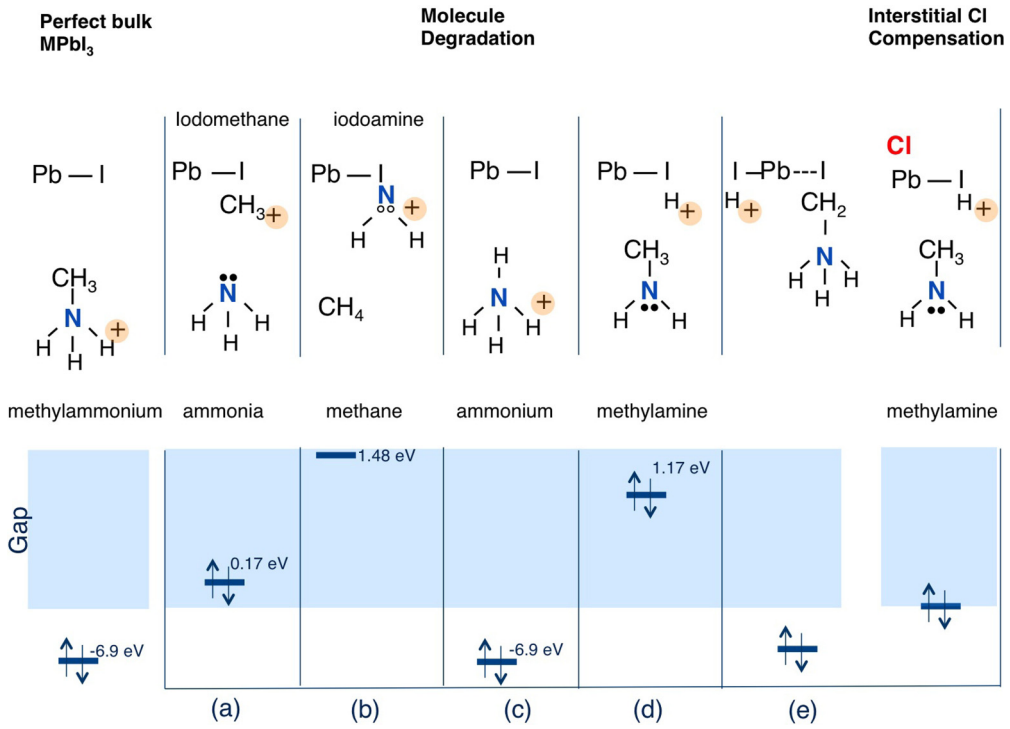

FIG. 6. (Color online) Scheme of the stable fragments considered in the present work under stoichiometric conditions. For each configuration the molecular levels closer to the band gap region are also indicated. In particular, amine groups display localized lone-pair HOMO and LUMO orbitals well into the band gap which are eventually removed after addition of interstitial Cl.

doublets at −9 eV and at −4.8 eV. The electronic orbitals relative to the doublet at −4.8 eV are the bond orbitals of the complex showing a strong hybridization between I($5p$) and C($2p$) atomic orbitals.

H. Effects of the p-type doping

In the stoichiometric dissociation processes described above the loss of a neutral M leaves the I($5p$) valence band manifold with one electronic vacancy. This hole is compensated when a dissociation fragment binds to a I atom (forming H–I, CH_3–I, NH_2–I, or CH_2NH_3–I complexes) so that no holes are present at the VBM.

Starting from these stoichiometric configurations (see Fig. 6), in order to explore the effect of p doping on the intragap localized states, we further enforced p-type conditions by subtracting electron charges from the supercell.

As illustrated by plots in Fig. 7 the behavior of N($2p$) lone pair levels is quite surprising. In p-type conditions these localized levels shift down below the VBM and maintain an almost full occupation. If—by an increase of hole concentration in the supercell—we shift further down the Fermi level, the lone-pair undergoes rigidly to the same energy shift, and again remains fully occupied.

An outstanding consequence then results from our simulations: amine lone-pair levels can stay in the gap as long as they are fully occupied or empty, but not if partially occupied, since in this case they regain full occupancy by shifting in energy below the VBM and thus taking one electron charge from the I($5p$) valence bands. According to these results it is thus impossible to have N($2p$) lone-pair levels with partial filling. As previously mentioned, the lack of in-gap partially filled states is in agreement with the arguments based on PL experiments of Refs. [12] and [19].

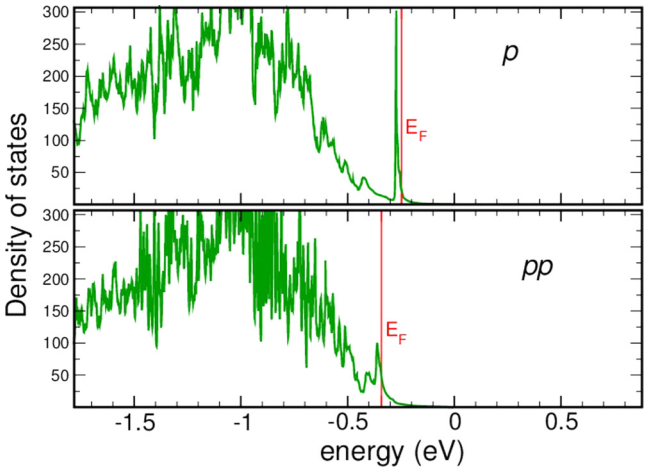

FIG. 7. (Color online) Density of states close to the VBM for two $MPbI_3$ supercells containing one methylamine at different hole doping concentrations. Top-panel: a bulk $MPbI_3$ with one methylammonium substituted by one methylamine (i.e., one H subtracted) in the 192-atom supercell. This corresponds to a hole doping concentration of 2.74×10^{20} cm^{-3}. Bottom panel: a bulk $MPbI_3$ plus a M-vacancy plus a M-to-methylamine substitution (2 holes per supercell). The 0 reference energy is placed at the VBM and the Fermi level value E_F has been computed with the linear tetrahedron method.

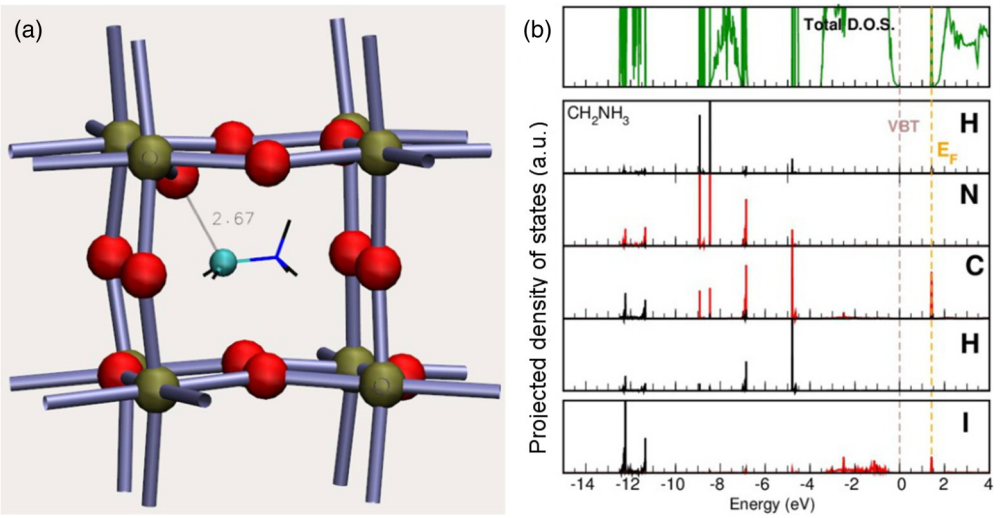

FIG. 8. (Color online) (a) Atomic structure of the $CH_2NH_3^+$–I complex in p-type conditions. (b) Electronic structure of the complex illustrated by the DOS projected on the atomic orbitals of the molecules. The Fermi level energy E_F is computed with the linear tetrahedron method.

A quite different behavior is obtained for the CH_2NH_3-I complex. As shown in Fig. 8, under p-doping conditions, this complex undergoes significant electronic and structural changes. The HOMO doublet, which in intrinsic conditions is a strongly covalent superposition of C($2p$) and I($5p$) orbitals, splits, in consequence of p doping, in a fully occupied C($2p$) singlet—laying about 5 eV below the VBM—and in a half-filled localized state inside the band gap—at about 1.4 eV above the VBM [36]. This result is coherent with EPR measurements in irradiated $MPbI_3$ [18] which indicate the presence of half-filled electronic orbitals derived by $CH_2NH_3^+$ ions.

In summary, according to our results N-derived and C-derived localized in-gap states behave quite differently: The former can never stay partially occupied in the band gap, and subtract electrons from the valence band if p-doping conditions are enforced; the latter, on the other hand, remains well within the band gap even if half occupied. We can understand this difference on the basis of the very high electronegativity of the p-doped N-H group. In comparison, the electronegativity of C-H molecules is much lower and these latter have thus the tendency to form hybridized bonds with I ions or alternatively strip H from neighboring M molecules.

Finally, the total energy comparison between perovskites including methylamine and $CH_2NH_3^+$ in the same p-type conditions (thus directly comparable having the same number of atoms in the simulation supercell) shows that the latter is 0.46 eV/f.u. higher in energy. Thus, the dissociation of methylammonium in methylamine should be regarded as the most probable source of in-gap localized defects in the perovskite.

I. Role of Cl in perovskites

A major conundrum concerns the capability of Cl to enhance the photoconversion properties of the perovskite; since the revealing of the conversion efficiency of these systems [1], the presence of Cl in solution with the reactants of the perovskite has been highlighted as a key ingredient to obtain power conversion efficiency (PCE) greater than 10%. This is somewhat surprising since on the one hand, the actual amount of Cl included in the perovskite was revealed to be not larger than a few percent and possibly accumulated at the interfaces [28,29]. On the other hand, it was realized that the isovalent Cl-I substitution could bring little effect on the fundamental electronic properties of the system [25]; in fact, several PL studies highlighted the fact that Cl could increase the lifetime and the related diffusion length of the perovskite by an order of magnitude [2], a result hardly understandable in terms of a few-percent I $\rightarrow$ Cl substitutions.

These considerations have motivated a thorough search of the possible mechanisms which could explain the role of Cl in the perovskites. At present, one of the most credited hypothesis focuses on the role of the interfaces where a significant concentration of Cl could be confined, thus effectively changing the photoabsorption properties [28,29].

An alternative explanation, very interesting in its simplicity, is based on the hypothesis that a certain amount of native defects present in the undoped stoichiometric perovskite could be removed from the gap by the inclusion of interstitial Cl, acting as a p-type dopant. An estimate based on purely radiative band-to-band recombination [7] showed that a reduction of defect concentration of about one order of magnitude can justify an increase of lifetime of the order of that found in PL experiments.

This scenario implies that: (i) native doping in the perovskite is n-type; (ii) interstitial Cl doping is somehow capable of eliminating the defect states laying in the band gap. In our description of methylammonium dissociations, we found that condition (i) is actually realized by two configurations characterized by HOMO levels well into the band gap (see a summary of results in Fig. 6).

In the following we will show that even the hypothesis (ii) is absolutely justified by our calculations, i.e., the inclusion of interstitial Cl always acts in a way to compensate the trap

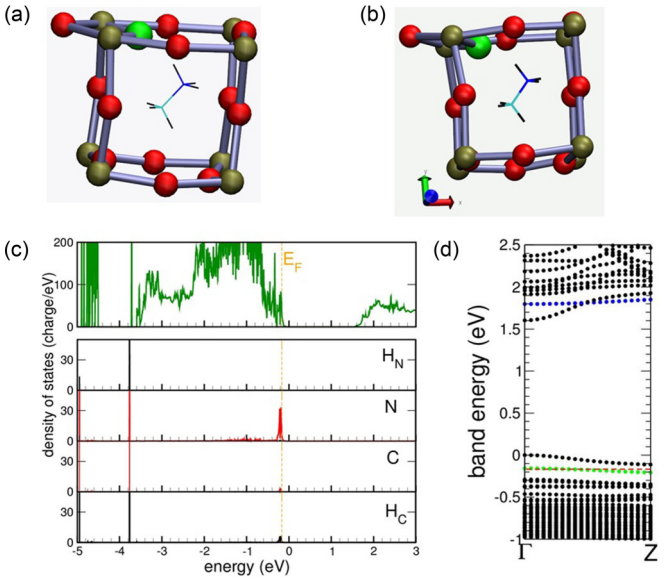

FIG. 9. (Color online) (a) Atomic structure obtained upon structural optimization after inclusion of one Cl in a bulk-like MPbI3 supercell; (b) atomic structure upon structural optimization with Cl included in a supercell after M dissociation in methylamine plus hydrogen iodide. In both cases, Cl ends up in the octahedral cage, binding with Pb atoms. (c) DOS relative to the system displayed in (b). The upmost panel is the total DOS, lower panel the DOS of the methylamine molecule, resolved per atoms. As usual red and black colors represent p and s states. (d): Band structure for the same system along Γ–Z. The green line is the HOMO of methylamine, the blue line a HI state, both laying within the band gap before Cl inclusion [Fig. 5(d)].

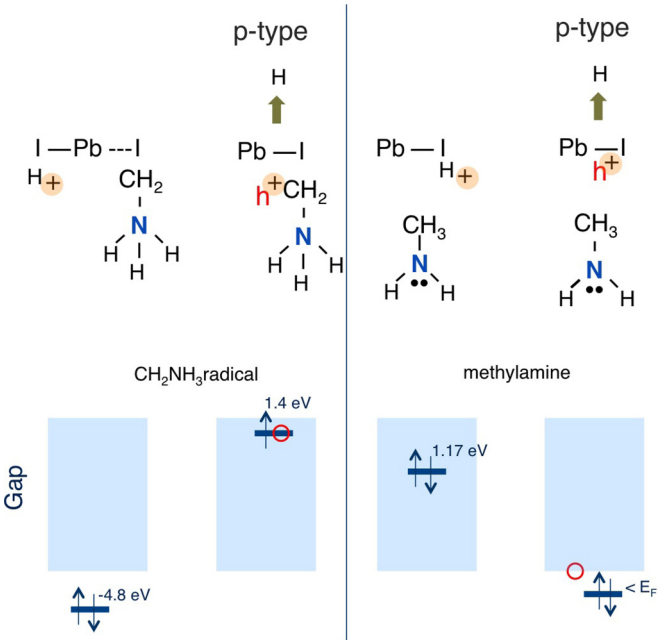

FIG. 10. (Color online) Schematic representations of the effects of p-type doping; (left) the molecular level of the methyl-type fragment is able to trap one hole and it forms a singly occupied level right in the gap; (right) the lone pair of the methylamine fragment is always doubly occupied, and shifts below the Fermi level in p-type conditions.

states and remove them from the band gap. We have simulated the inclusion of a Cl atom in the perovskite, together with the most interesting end products of methylammonium, for various Cl starting positions.

The inclusion of one Cl in our 16 f.u. supercells corresponds to a 2% additional concentration with respect to the I atoms, in line with the PL estimates of defect concentration. Interestingly, we found a rather universal behavior for the interstitial Cl, i.e., scarcely dependent on the initial atomic configurations: In all the cases, Cl migrates into the octahedral cage, bonding with one Pb and distorting the Pb-I octahedral cage; in Figs. 9(a) and (b) we report the final structure for two different simulations, one with an additional Cl atom included in the bulk $MPbI_3$ perovskite, and the other with a Cl included together with CH_3NH_2 and HI as products of the methylammonium dissociation. The two atomic structures in the region around Cl are quite similar, with Cl moving close to a Pb and sharing the ligand position with one I ion.

In this way Cl($3p$) states are hybridized with the I($5p$) valence states, thus effectively decreasing the n-type concentration by one electron per Cl. In Fig. 9 we report DOS and band energies relative to the relaxed structure with one CH_3NH_2 plus HI plus Cl. The HOMO state of methylamine, which in the absence of Cl was well into the band gap, is now located just below the VBM, i.e., the inclusion of Cl cleans up the band gap from its occupied localized states.

This *cleaning* mechanism is rather transparent: Cl grabs an electron from the in-gap lone pair, which then falls down in energy as a consequence of the subtracted electrostatic repulsion. Furthermore, the p-type states of Cl spreads through the I($5p$) valence band region, without introducing any relevant change in the total DOS, i.e., the basic electronic properties of the perovskite are not disrupted by the interstitial Cl, at least for the 2% concentration examined here. We emphasize that this mechanism is quite general: Any n-type dopant, whatever the source, will be compensated by an equal concentration of interstitial Cl subtracting one electron from the valence band manifold.

IV. CONCLUSIONS

In summary, we have studied by first-principles calculations the effect in the perovskites of various molecular defects. We have focused our analysis on those which can be obtained by the dissociation or fragmentation of methylammonium. For these defects the formation energies calculated by total energy differences range from about 2 eV up to 3.2 eV. Accordingly their concentration is expected to be low under thermal equilibrium conditions, but it can eventually increase out of equilibrium, i.e., during synthesis or as a result of chemical contamination.

Our results demonstrate that some of these defects form (either completely filled or empty) localized levels inside the band gap, in particular those related to N($2p$) lone pairs present in ammonia and methylamine molecules derived from methylammonium dissociation. An overall account of these defects is schematically summarized in Fig. 6: While the

electronic states of the M^{1+} molecule in the bulk perovskite lie far beyond or above the relevant band gap extremes, these molecules display either HOMO or LUMO states well within the band gap (specifically, the ammonia HOMO 0.17 eV above the VBM, and the methylamine HOMO and LUMO 1.17 eV and 1.48 eV above VBM, respectively).

Also, we have shown that the amine lone pairs localized in the band gap are always either full or empty, since any attempt to extract an electron from the in-gap HOMO state results in a sudden falling of this state below the VBM. In other words, their fractionally occupied states are never stable within the band gap. This result is in striking agreement with the interpretations of the steady-state PL experiments carried out in Ref. [12].

At variance with amines, fragments having a C($2p$) lone pair like CH_2NH_3 or CH_3 can form stable complexes by binding to I ions, but, as long as stoichiometric conditions are retained, their HOMO levels always remain well below the VBM. However, in p-type conditions the orbital related to C-I bond remains singly occupied thus moving into the band gap; this is in agreement with EPR evidences, reported in Ref. [18], of half-filled orbitals derived by the CH_2NH_3 radical. Results for p-type conditions are summarized in Fig. 10.

Furthermore, we have analyzed the inclusion of interstitial Cl in the perovskite. Our results show that an amount of 2% interstitial Cl is capable of removing from the band gap an equal amount of N-derived lone-pair HOMO states of methylamine or ammonia, and at the same time does not disrupt the fundamental electronic properties of the perovskite. Our results build a sound conceptual fundament to the observed enhancement of lifetime and diffusion length caused by the inclusion of Cl in the solution processing of the perovskite.

ACKNOWLEDGMENTS

The authors acknowledge financial support by CompuNet, Istituto Italiano di Tecnologia (IIT), by Regione Autonoma della Sardegna under L. R. 7/2007 (CRP- 24978 and CRP-18013), by Consiglio Nazionale delle Ricerche (Progetto Premialitá RADIUS), by Fondazione Banco di Sardegna Project No. 5794 and No. 7454. They also acknowledge computational support by CINECA (Casalecchio di Reno, Italy) and CRS4 (Loc. Piscina Manna, Pula, Italy).

[1] M. M. Lee, J. Teuscher, T. Miyasaka, T. N. Murakami, and H. J. Snaith, Efficient hybrid solar cells based on meso-superstructured organometal halide perovskites, Science **338**, 643 (2012).

[2] S. D. Stranks, G. E. Eperon, G. Grancini, C. Menelaou, M. J. P. Alcocer, T. Leijtens, L. M. Herz, A. Petrozza, and H. J. Snaith, Electron-hole diffusion lengths exceeding 1 micrometer in an organometal trihalide perovskite absorber, Science **342**, 341 (2013).

[3] G. Xing, N. Mathews, S. Sun, S. S. Lim, Y. M. Lam, M. Grätzel, S. Mhaisalkar, and T. C. Sum, Long-range balanced electron- and hole-transport lengths in organic-inorganic $CH_3NH_3PbI_3$, Science **342**, 344 (2013).

[4] J. Burschka, N. Pellet, S.-J. Moon, R. Humphry-Baker, P. Gao, M. K. Nazeeruddin, and M. Grätzel, Sequential deposition as a route to high-performance perovskite-sensitized solar cells, Nature (London) **499**, 316 (2013).

[5] G. Xing, N. Mathews, S. S. Lim, N. Yantara, X. Liu, D. Sabba, M. Grätzel, S. Mhaisalkar, and T. C. Sum, Low-temperature solution-processed wavelength-tunable perovskites for lasing, Nat. Mater. **13**, 476 (2014).

[6] E. Mosconi, A. Amat, M. K. Nazeeruddin, M. Grätzel, and F. De Angelis, First-principles modeling of mixed halide organometal perovskites for photovoltaic applications, J. Phys. Chem. C **117**, 13902 (2013).

[7] A. Filippetti and A. Mattoni, Hybrid perovskites for photovoltaics: Insights from first principles, Phys. Rev. B **89**, 125203 (2014).

[8] A. Filippetti, P. Delugas, and A. Mattoni, Radiative recombination and photoconversion of methylammonium lead iodide perovskite by first principles: Properties of an inorganic semiconductor within a hybrid body, J. Phys. Chem. C **118**, 24843 (2014).

[9] W.-J. Yin, T. Shi, and Y. Yan, Unique properties of Halide perovskites as possible origins of the superior solar cell performance, Adv. Mater. **26**, 4653 (2014).

[10] W.-J. Yin, J.-H. Yang, J. Kang, Y. Yan, and S.-H. Wei, Halide perovskite materials for solar cells: A theoretical review, J. Mater. Chem. A **3**, 8926 (2014).

[11] S. De Wolf, J. Holovsky, S.-J. Moon, P. Lper, B. Niesen, M. Ledinsky, F.-J. Haug, J.-H. Yum, and C. Ballif, Organometallic halide perovskites: Sharp optical absorption edge and its relation to photovoltaic performance, J. Phys. Chem. Lett. **5**, 1035 (2014).

[12] M. Saba, M. Cadelano, D. Marongiu, F. Chen, V. Sarritzu, N. Sestu, C. Figus, M. Aresti, R. Piras, A. Geddo Lehmann, C. Cannas, A. Musinu, F. Quochi, A. Mura, and G. Bongiovanni, Correlated electron-hole plasma in organometal perovskites, Nat. Commun. **5**, 5049 (2014).

[13] V. D'Innocenzo, G. Grancini, M. J. P. Alcocer, A. R. S. Kandada, S. D. Stranks, M. M. Lee, G. Lanzani, H. J. Snaith, and A. Petrozza, Excitons versus free charges in organo-lead tri-halide perovskites, Nat. Commun. **5**, 3586 (2014).

[14] K. Tvingstedt, O. Malinkiewicz, A. Baumann, C. Deibel, H. J. Snaith, V. Dyakonov, and H. J. Bolink, Radiative efficiency of lead iodide based perovskite solar cells, Sci. Rep. **4**, 6071 (2014).

[15] A. Marchioro, J. Teuscher, D. Friedrich, M. Kunst, R. van de Krol, T. Moehl, M. Gratzel, and J.-E. Moser, Unravelling the mechanism of photoinduced charge transfer processes in lead iodide perovskite solar cells, Nat. Photon. **8**, 250 (2014).

[16] V. Roiati, S. Colella, G. Lerario, L. De Marco, A. Rizzo, A. Listorti, and G. Gigli, Investigating charge dynamics in halide perovskite-sensitized mesostructured solar cells, Energy Environ. Sci. **7**, 1889 (2014).

[17] J. Kim, S.-H. Lee, J. H. Lee, and K.-H. Hong, The role of intrinsic defects in methylammonium lead iodide perovskite, J. Phys. Chem. Lett. **5**, 1312 (2014).

[18] I. A. Shkrob and T. W. Marin, Charge trapping in photovoltaically active perovskites and related halogenoplumbate compounds, J. Phys. Chem. Lett. **5**, 1066 (2014).

[19] T. Leijtens, S. D. Stranks, G. E. Eperon, R. Lindblad, E. M. J. Johansson, I. J. McPherson, H. Rensmo, J. M. Ball, M. M. Lee, and H. J. Snaith, Electronic properties of meso-superstructured and planar organometal halide perovskite films: Charge trapping, photodoping, and carrier mobility, ACS Nano **8**, 7147 (2014).

[20] B. Conings, L. Baeten, C. De Dobbelaere, J. D'Haen, J. Manca, and H.-G. Boyen, Perovskite-based hybrid solar cells exceeding 10% efficiency with high reproducibility using a thin film sandwich approach, Adv. Mater. **26**, 2041 (2014).

[21] W.-J. Yin, T. Shi, and Y. Yan, Unusual defect physics in $CH_3NH_3PbI_3$ perovskite solar cell absorber, Appl. Phys. Lett. **104**, 063903 (2014).

[22] A. Buin, P. Pietsch, J. Xu, O. Voznyy, A. H. Ip, R. Comin, and E. H. Sargent, Materials processing routes to trap-free halide perovskites, Nano Lett. **14**, 6281 (2014).

[23] H.-S. Duan, H. Zhou, Q. Chen, P. Sun, S. Luo, T.-B. Song, B. Bob, and Y. Yang, The identification and characterization of defect states in hybrid organic-inorganic perovskite photovoltaics, Phys. Chem. Chem. Phys. **17**, 112 (2014).

[24] M. H. Du, Efficient carrier transport in halide perovskites: Theoretical perspectives, J. Mater. Chem. A **2**, 9091 (2014).

[25] S. Colella, E. Mosconi, P. Fedeli, A. Listorti, F. Gazza, F. Orlandi, P. Ferro, T. Besagni, A. Rizzo, G. Calestani, G. Gigli, F. De Angelis, and R. Mosca, $MaPbI_{3-x}Cl_x$ mixed halide perovskite for hybrid solar cells: The role of chloride as dopant on the transport and structural properties, Chem. Mater. **25**, 4613 (2013).

[26] P. Giannozzi, S. Baroni, N. Bonini, M. Calandra, R. Car, C. Cavazzoni, D. Ceresoli, G. L. Chiarotti, M. Cococcioni, I. Dabo, A. Dal Corso, S. de Gironcoli, S. Fabris, G. Fratesi, R. Gebauer, U. Gerstmann, C. Gougoussis, A. Kokalj, M. Lazzeri, L. Martin-Samos, N. Marzari, F. Mauri, R. Mazzarello, S. Paolini, A. Pasquarello, L. Paulatto, C. Sbraccia, S. Scandolo, G. Sclauzero, A. P. Seitsonen, A. Smogunov, P. Umari, and R. M. Wentzcovitch, QUANTUM ESPRESSO: A modular and open-source software project for quantum simulations of materials, J. Phys.: Condens. Matter **21**, 395502 (2009).

[27] D. Vanderbilt, Soft self-consistent pseudopotentials in a generalized eigenvalue formalism, Phys. Rev. B **41**, 7892(R) (1990).

[28] E. Mosconi, E. Ronca, and F. De Angelis, First-principles investigation of the TiO_2/organohalide perovskites interface: The role of interfacial chlorine, J. Phys. Chem. Lett. **5**, 2619 (2014).

[29] S. Colella, E. Mosconi, G. Pellegrino, A. Alberti, V. L. P. Guerra, S. Masi, A. Listorti, A. Rizzo, G. G. Condorelli, F. De Angelis, and G. Gigli, Elusive presence of chloride in mixed halide perovskite solar cells, J. Phys. Chem. Lett. **5**, 3532 (2014).

[30] C. Motta, F. El-Mellouhi, S. Kais, N. Tabet, F. Alharbi, and S. Sanvito, Revealing the role of organic cations in hybrid halide perovskite $CH_3NH_3PbI_3$, Nat. Commun. **6**, 7026 (2015).

[31] A. Stroppa, D. Di Sante, P. Barone, M. Bokdam, G. Kresse, C. Franchini, M.-H. Whangbo, and S. Picozzi, Tunable ferroelectric polarization and its interplay with spin–orbit coupling in tin iodide perovskites, Nat. Commun. **5**, 5900 (2014).

[32] A. Stroppa, C. Quarti, F. De Angelis, and S. Picozzi, Ferroelectric polarization of $CH_3NH_3PBI_3$: A detailed study based on density functional theory and symmetry mode analysis, J. Phys. Chem. Lett. **6**, 2223 (2015).

[33] J. Even, L. Pedesseau, J.-M. Jancu, and C. Katan, Importance of spin-orbit coupling in hybrid organic/inorganic perovskites for photovoltaic applications, J. Phys. Chem. Lett. **4**, 2999 (2013).

[34] P. Umari, E. Mosconi, and F. De Angelis, Relativistic GW calculations on $CH_3NH_3PbI_3$ and $CH_3NH_3SnI_3$ perovskites for solar cell applications, Sci. Rep. **4**, 4467 (2014).

[35] T. Baikie, Y. Fang, J. M. Kadro, M. Schreyer, F. Wei, S. G. Mhaisalkar, M. Graetzel, and T. J. White, Synthesis and crystal chemistry of the hybrid perovskite $(CH_3NH_3)PbI_3$ for solid-state sensitised solar cell applications, J. Mater. Chem. A **1**, 5628 (2013).

[36] See Supplemental Material at http://link.aps.org/supplemental/10.1103/PhysRevB.92.045301 for more details and additional figures.